COMPDYN 2025
10th ECCOMAS Thematic Conference on
Computational Methods in Structural Dynamics and Earthquake Engineering
M. Papadrakakis, M. Fragiadakis (eds.)
Rhodes Island, Greece, 15-18 June 2025

3D NUMERICAL INVESTIGATION OF THE SEISMIC RESPONSE OF A SHALLOW TUNNEL CROSSING A TOPOGRAPHICALLY COMPLEX AREA

Annamaria di Lernia[1], Gaetano Falcone[2], Leonardo Todisco[3] and Gaetano Elia[1]

[1] Department of Civil, Environmental, Land, Building Engineering and Chemistry (DICATECh),
Politecnico di Bari
via Orabona 4, 70125 Bari, Italy
e-mail: {annamaria.dilernia, gaetano.elia}@poliba.it

[2] Department of Civil, Building and Environmental Engineering (DICEA),
Università di Napoli Federico II
via Claudio 21, Napoli, 80125, Italy
gaetano.falcone@unina.it

[3] School of Civil Engineering, Universidad Politécnica de Madrid
calle Prof. Aranguren 3, Madrid, 28040, Spain
leonardo.todisco@upm.es

Abstract

The seismic risk assessment of tunnels is of fundamental importance, given the great role played by this class of infrastructures in urban areas, as well as in interurban transportation networks. It entails the quantitative evaluation of the seismic-induced damages on these underground structures and, in general, the estimation of their resilience during and after earthquakes. Within this context, the paper presents a three-dimensional (3D) numerical investigation of the seismic response of a shallow twin-tunnel crossing a topographically complex area. The numerical study is inspired by the old Alvaro tunnel, located at the toe of the Costa del Canneto slope (Matera, Italy) in the South of Italy. The 3D finite element model is initialized by simulating a realistic tunnel excavation sequence, performed with conventional methods and subsequent tunnel lining installation, within a heterogeneous subsoil deposit, implementing a shear wave velocity profile variable with depth. The soil behavior is described through the isotropic hardening elasto-plastic hysteretic constitutive model HSsmall, while the tunnel lining is modelled using a linear elastic law. The results emphasize the capability of the 3D modelling approach to estimate the distribution of the lining forces along the whole infrastructure, accounting for the complex topographic conditions, the possible interaction between the two tunnels and the multi-directionality of the seismic motion. Moreover, the calculated damage index distribution shows that, depending on the amount of assumed steel reinforcement, (i) the damages are observed on the lining already at the end of the tunnel construction stage; (ii) the occurrence of an earthquake may significantly aggravate the induced-damage distribution.

Keywords: Dynamic slope-tunnel interaction, 3D FE modelling, shallow tunnels, nonlinear analyses, earthquake-induced damage

1 INTRODUCTION

In recent years, the increasing relevance for civil society of existing infrastructures located in urban areas, as well as integrated in interurban transportation networks, is urging the assessment of their vulnerability related to natural disasters, such as landslides and earthquakes [1]. Among these strategic infrastructures, tunnels are considered "lifeline" utilities, since their continuous functionality is of vital importance. The damages induced by their interaction with unstable slopes or due to earthquakes need to be appropriately estimated for a quantitative evaluation of their resilience during and after natural disasters.

Several methods, i.e. analytical, experimental and numerical, may be adopted for the investigation of the seismic response of tunnels, each characterized by different levels of complexity and requiring several assumptions and simplifications. The availability of high-capacity computing facilities allows nowadays for the construction of sophisticated three-dimensional (3D) numerical models, implementing complex geometries and advanced constitutive models [2,3]. The adoption of such 3D numerical models can be important when dealing with the assessment of the seismic response of tunnels crossing areas characterized by complex site conditions [4].

Within this context, the paper presents a nonlinear 3D numerical investigation of the seismic response of a shallow tunnel (i.e. characterized by a mean value of the cover to diameter ration lower than 2) crossing a topographically complex area. The numerical study is inspired by the case of the Alvaro twin-tunnel, located at the toe of the Costa del Canneto slope (Matera, Italy) in the South of Italy [5,6], which has been selected as representative of those cases of existing strategic infrastructure within complex topographic contexts. The impact on the tunnel lining force distribution of the topographical model adopted to simulate the sloping area has been already studied by Falcone *et al*. [7] through 3D numerical simulations of two slope models with different mesh refinements. The results enlightened how the accuracy of the topographic model may considerably affect the lining forces predicted along the tunnel under both static and dynamic conditions. In a recent paper by the same Authors [8], the influence of the tunnel construction sequence and the subsoil conditions on the lining force distribution has been investigated through 3D finite element (FE) simulations of the dynamic soil-tunnel interaction. Due to several uncertainties on the soil characteristics, the geometrical and mechanical properties of the tunnel lining and the excavation sequence adopted during its construction, two realistic tunnel excavation strategies have been modelled considering two subsoil conditions, one homogeneous and one heterogeneous in terms of shear wave velocity variation with depth. In these analyses, the soil behavior has been simulated using the isotropic hardening elasto-plastic HSsmall model [9,10], while a linear elastic law has been assumed for the tunnel lining response. The results have shown the insignificant influence of the tunnel construction sequence on the lining force distribution, both at the end of the construction and at the end of the earthquake. Conversely, the variable shear wave profile of the soil deposit is deemed to be responsible for an overall increase in the lining forces and a different distribution of their maximum values along the tunnel, due to the greater tendency of the soil to deform at shallower depths.

The present work aims at evaluating the damage distribution on the tunnel lining induced by both the static loading at the end of the tunnel construction stage and the occurrence of an earthquake, by analyzing the results of 3D FE nonlinear analyses of the same case study. The numerical model, initialized by simulating a realistic tunnel excavation sequence within a heterogeneous subsoil deposit, is then subjected to the two horizontal components of an earthquake. The level of tunnel damage is described by a damage index (DI), expressing the exceedance of the lining strength capacity according to the approach proposed by [11].

2 THE ALVARO TUNNEL CASE STUDY

Built in 1969-1970, the Alvaro tunnel is a twin-tube shallow infrastructure on the Basentana State Road, crossing the toe of the Costa del Canneto area close to the town of Ferrandina (Matera, Italy - Figure 1a). The tunnel runs parallel to the Basento river, on the right slope of its valley (Figure 1b), lying within a blue-grey clay deposit. The Costa del Canneto area is characterized by a complex uneven topography, making the area susceptible to seismic amplification and landslides (Figure 1b). A main slope of 11° average inclination can be identified on the right bank of the Basento river, while local slopes characterized by inclinations in the range of 10°–30° are present in the entire area.

The Alvaro tunnel is characterized by a reinforced concrete (RC) horseshoe-like cross section of equivalent diameter D of about 11 m and thickness of 0.9 m. The right tube is 690 m long, while the left tube has a length of 640 m.

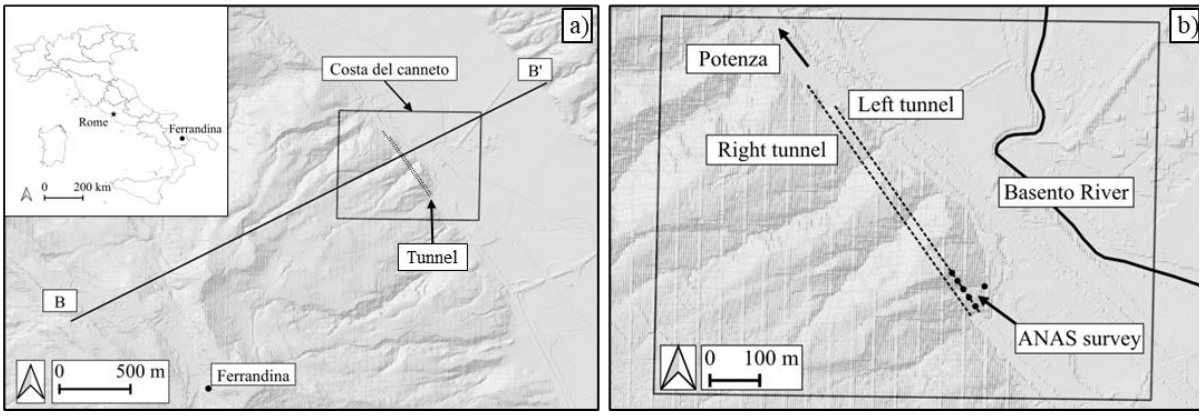

Figure 1: a) Location of the Costa del Canneto area and b) close-up of the Alvaro tunnel (modified after [8]).

The characterization of both the soil surrounding the tunnel and the lining has been performed based on the survey (Figure 1b) carried out by ANAS-Basilicata in 2014 [12], which included boreholes, triaxial and simple shear tests on undisturbed soil samples, flat jack and compression tests on concrete cubic specimens of the tunnel secondary lining. The main properties of the blue-grey clays and the characteristics of the tunnel lining are listed in Table 1.

More specifically, the compressive strength, f_{ck}, of the concrete cubic specimens, estimated by averaging the results of the compression tests, is about 30 MPa, corresponding to the C25/30 concrete class according to the Italian building code [13]. The corresponding Young modulus, E, has been assumed equal to 31.5 GPa. In absence of direct information, the steel reinforcement yield stress, f_{yk}, has been assumed equal to 391 MPa, as typically observed for similar infrastructures of the same age located within the same area. Since the tunnel was constructed using conventional excavation methods, a primary support was required during the excavation stages. As no direct information is available, the primary lining has been assumed to consist of steel reinforcing elements embedded in fiber-reinforced shotcrete.

The clay properties summarized in Table 1 have been determined as average values of the available laboratory data. It should be mentioned that they fall within the range retrieved from the available literature [5,6,14], according to which the unit weight of the blue-grey clays varies between 18 kN/m^3 and 21 kN/m^3, the effective cohesion, c', ranges from 15 kPa to 30 kPa, the effective friction angle, φ', covers the interval 17°–30°, the Plasticity Index, PI, ranges between 15% and 30%, while the overconsolidation ratio, R_0, is in the range 1.8–2.7.

	Blue-grey clays	Secondary lining
γ [kN/m^3]	20	25
c' [kPa]	22	-
φ' [°]	25	-
c_u [kPa]	223	-
PI [%]	15	-
E [GPa]	-	31.5
f_{ck} [MPa]	-	25
f_{yk} [MPa]	-	391

Table 1: Properties of the blue-grey clays surrounding the tunnel and the secondary lining.

Due to the lack of direct experimental data, the dynamic characteristics of the blue-grey clay deposit have been assumed to be described by the Viggiani and Atkinson (V&A) equation [15] for the shear wave velocity profile with depth (Figure 2a) and by the Darendeli decay curves [16] for the cyclic response in terms of normalized secant shear stiffness G/G_0 (Figure 2b) and damping ratio D (Figure 2c). In the V&A formulation, the parameters A, m, and n have been defined equal to 1900, 0.2, and 0.7, respectively, as a function of PI=15%, while R_0 has been set equal to 2.0. As for the G/G_0 and D curves, those associated to a PI equal to 15%, cyclic loading frequency of 1 Hz, number of cycles equal to 5, overconsolidation ratio of 2 and mean effective stress of 733 kPa have been chosen from [16].

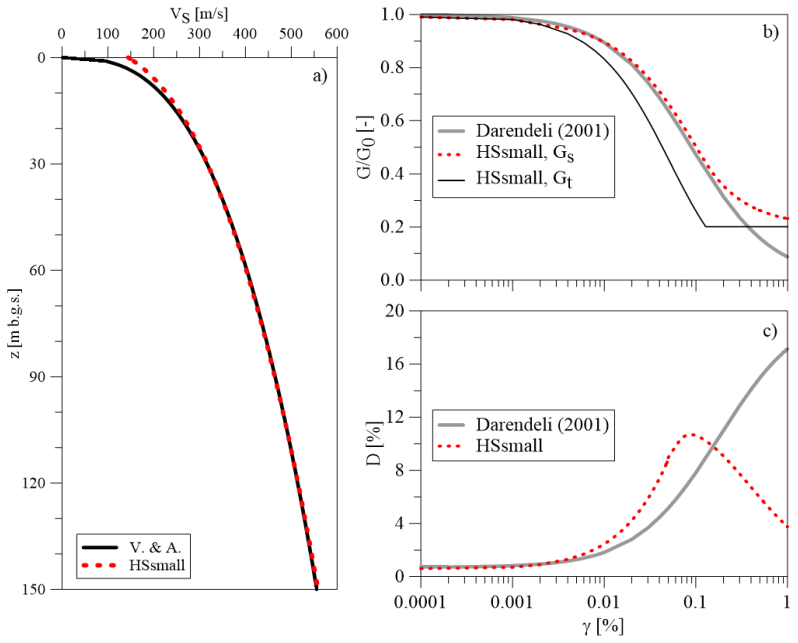

Figure 2: Calibration of the HSsmall model based on a) $V_s(z)$ profile following the V&A equation [15]; b) normalized shear stiffness $G(\gamma)/G_0$ and c) damping ratio $D(\gamma)$ curves obtained from [16].

3 NUMERICAL MODELLING OF THE SLOPE-TUNNEL INTERACTION

3.1 Implementation of the 3D FE numerical model

The slope-tunnel interaction under both static and dynamic conditions has been investigated through 3D numerical simulations performed with the FE code PLAXIS 3D [17]. The numerical model incorporates an accurate representation of the real topography of the area and accounts for the presence of the twin-tube tunnel (Figure 3). The 3D FE mesh consists of about 230,000 10-noded tetrahedral elements, with a coarseness adjusted to ensure a distance between two consecutive nodes smaller than approximately one-eighth of the smallest wavelength of the seismic excitation ($\lambda_S=V_S/f_{max}$), where V_S is the shear wave velocity of the soil and f_{max} is the maximum frequency content of the input signal [18]. A greater mesh refinement is adopted for the soil surrounding the tunnel, to obtain a more accurate prediction of its response in this area. The tunnels, characterized by a horseshoe-like transverse section (Figure 3b), have been implemented as plate elements (Figure 3c) of different mechanical characteristics depending on whether they represent the primary or the secondary lining. The tunnel lining and the surrounding soil have been assumed purely bonded, meaning that the soil-lining interface transfers very high friction forces and the relative displacement between the two materials is negligible.

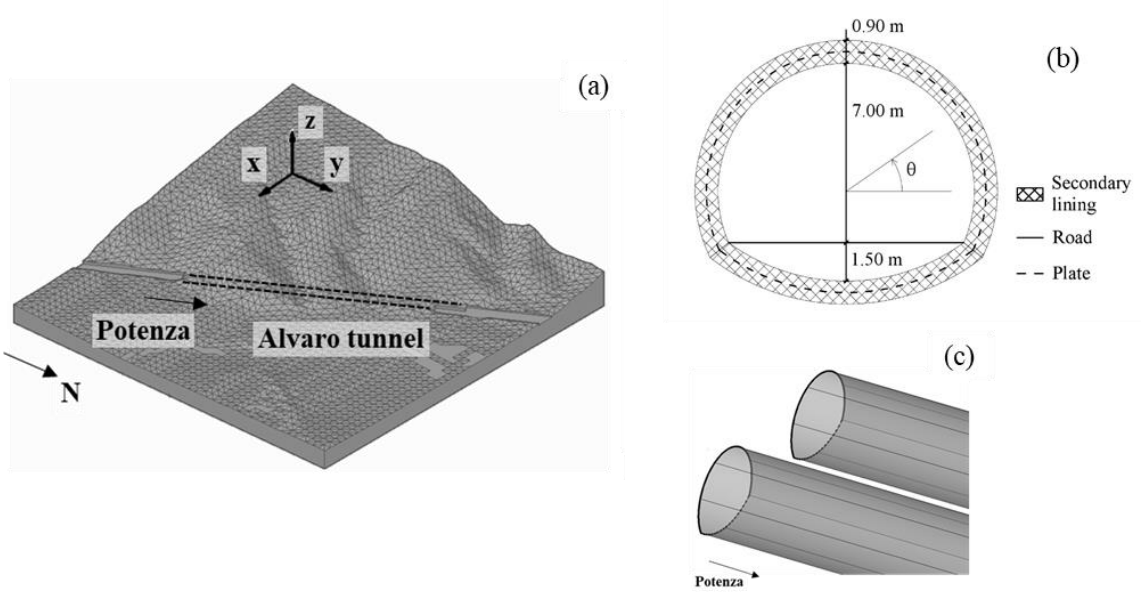

Figure 3: a) 3D numerical model of the Costa del Canneto area including the Alvaro twin-tunnel; b) transversal section and c) sketch up of the tunnels implemented in the numerical model.

The FE analysis consists of a first plastic stage devoted to the stress state initialization performed adopting the gravity loading procedure, in which the initial stress state is generated by increasingly applying the self-weight of the soil. Then, a set of static plastic phases have been executed to simulate the tunnel construction stages. Once the tunnels have been fully constructed, the dynamic analysis has been carried out by simultaneously applying both the horizontal components of a selected input motion. Given the lack of specific information about the hydraulic regime within the slope, the water table has been located at the base of the numerical model to reduce the degree of complexity of the simulations, while drained conditions have been implemented for both the static and dynamic stages.

The simulation of the tunnel excavation with conventional methods and subsequent lining installation has been carried out implementing the following construction sequence: (*i*)

excavating the soil for a length of 3 m, during which the hole is unsupported; (*ii*) installing the primary lining at a distance of 3 m from the excavation front; (*iii*) installing the secondary lining at a distance equal to approximately three times the tunnel diameter as the front progressively advances. More specifically, the unsupported excavation front advances for a length of 3 m per step, followed by the activation of the primary lining. Once the primary lining is completely activated for the total length of 30 m, the secondary lining starts to be installed at the distance of (30 + 3) m from the front. A total of 246 plastic stages have been set for the construction of the right tube, longer than the left tube, for which only 226 plastic stages are necessary to complete its construction.

During the static stages, standard boundary conditions have been adopted. Free-field boundary conditions have been applied to the vertical sides of the model during the dynamic stage, simulating the propagation of waves into the far field domain with minimum reflection at the boundary, whereas the compliant base has been applied at the bottom of the model to simulate the wave dissipation into the deeper soil layers with minimal reflection at the lower boundary. This condition allows the propagation of the upgoing reference signals recorded at the outcropping bedrock as input motions.

The input motion has been selected based on the seismic hazard of the Costa del Canneto site, considering a reference response spectrum defined for a return period of 1898 years and contemplating the class of use of tunnels for a limit state of life safety (Figure 4a). The reference seismic motions, selected to be compatible with the target response spectrum and scaled to the PGA of the site equal to 0.24 g, are the NS and EW components of the earthquake recorded at Cascia (PG, Italy) on the 14th October 1997 with M=5.6 (Figure 4b and c). The acceleration time histories, applied at the base of the 3D model, are characterized by a duration of 10 s and have been filtered to a maximum frequency, f_{max}, of 15 Hz.

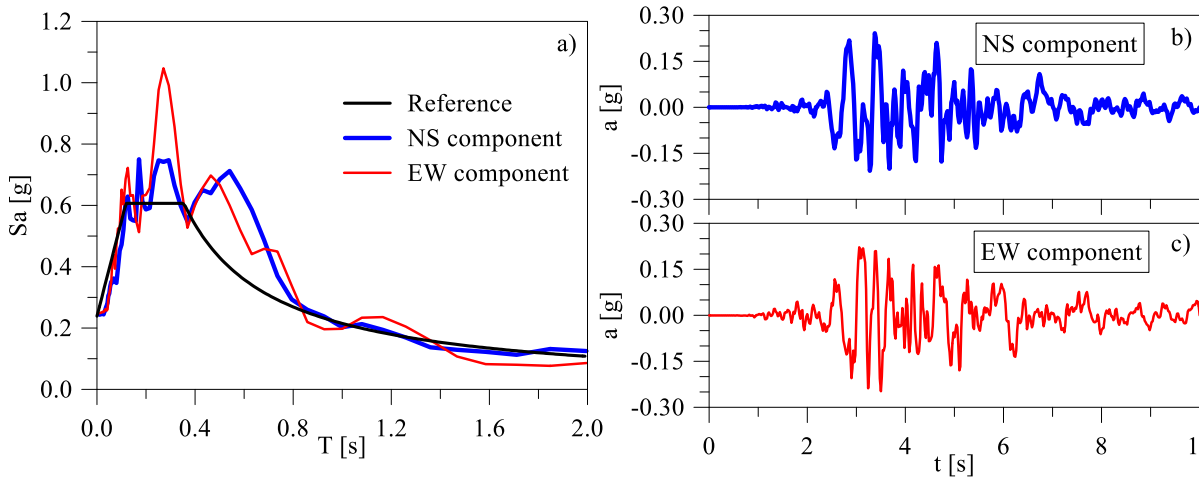

Figure 4: a) response spectra and b-c) acceleration time histories of the two components of the seismic motion recorded at Cascia (PG, Italy).

3.2 Soil and tunnel mechanical properties

The blue-gray clay behavior has been described by the HSsmall constitutive model, calibrated to replicate the cyclic soil response and the shear wave velocity profile reported in Figure 2. Specifically, the parameter $\gamma_{0.7}$, representing the shear strain at which the secant shear stiffness reduces to about 70% of its initial value, and the ratio G_0^{ref}/G_{ur}^{ref} have been determined to

obtain the best fitting of the G/G_0 curve, while the parameters G_0^{ref} and m have been chosen to fit the V_S profile. The stiffness parameters E_{50}^{ref} and E_{oed}^{ref} have been assumed to be three times lower the elastic unloading-reloading stiffness modulus E_{ur}^{ref}, this latter related to the unloading-reloading shear stiffness modulus G_{ur}^{ref}, defined as a function of G_0^{ref}/G_{ur}^{ref} (set equal to 5) through the Poisson's ratio for unloading-reloading ν_{ur}. The HSsmall parameters are summarized in Table 2. A small amount of Rayleigh damping [19] has been included in the FE dynamic simulations to provide energy dissipation in the very small strain range, not covered by the HSsmall model. The control frequencies f_m and f_n have been set equal to 1 Hz and 10 Hz, respectively, for a target damping D^* of 0.1%.

Parameter	Description	Value
c' [kPa]	Effective cohesion	22
φ' [°]	Effective friction angle	25
ψ [°]	Dilatancy angle	0
E_{50}^{ref} [kPa]	Reference secant stiffness in standard drained triaxial test	16.45·E3
E_{oed}^{ref} [kPa]	Reference tangent stiffness for primary oedometer loading test	16.45·E3
E_{ur}^{ref} [kPa]	Reference unloading/reloading stiffness at engineering strains	49.34·E3
ν_{ur} [-]	Poisson's ratio for unloading/reloading	0.25
G_0^{ref} [kPa]	Reference shear modulus at very small strains	98.68·E3
$\gamma_{0.7}$ [%]	Shear strain at which $G_S = 0.722 \cdot G_0^{ref}$	4·E-4
m [-]	Power for the stress-level dependency of stiffness	0.75
p'_{ref} [kPa]	Reference stress for stiffness	100
R [-]	Failure ratio	0.9

Table 2: HSsmall model parameters.

The blue-grey clay layer is underlain by a 0.5 m thick layer of bedrock, modelled as a linear visco-elastic material, with a total unit weight of 20 kN/m^3, a shear wave velocity V_S of 800 m/s, and Poisson's ratio equal to 0.25. A damping ratio of 0.01% has been implemented through the Rayleigh formulation with the same control frequencies adopted for the blue-grey clay layer.

Both the primary and the secondary linings have been implemented as linear elastic plate elements, characterized by different mechanical and geometrical properties. In particular, the primary lining, described by a homogenized material composed of two beams spaced 1 m apart and 0.25 m of C20/25 class shotcrete, is implemented with a thickness of 0.25 m, a unit weight of 20 kN/m^3 and a Young modulus of 35 MPa. The secondary lining of the tunnels has been modelled through a 0.9 m thick plate, with a unit weight of 25 kN/m^3 and a Young modulus equal to 31.5 GPa.

4 RESULTS AND DISCUSSION

The numerical results are investigated in terms of lining forces, i.e. axial force N2 and bending moment M11, retrieved in correspondence of four transversal sections crossing the right tunnel at the distance p equal to 150 m, 250 m, 350 m and 550 m (where p is the distance from the south-east portal of the tunnel). Positive values of the normal forces refer to tensile states, while negative values are representative of compression states. Positive values of the bending moments refer to the compression of the inner fibres, while negative values are indicative of the extension of the inner fibres. These lining forces are illustrated in Figure 5 considering the

ultimate M_R-N_R interaction diagram, constructed assuming different possible percentage of steel reinforcement in the cross section. The amount of reinforcement is expressed in terms of the ratio A_S/A, where A_S is the area of the total steel and A is the gross area of concrete. Due to the lack of direct information, three hypotheses on the ratio A_S/A have been made, i.e. 0% (absence of reinforcement), 0.5% and 1%, considered reasonable amounts of reinforcements for shallow tunnels. The concrete rectangular section is 1 m wide and 0.9 m thick and is characterised by a concrete cover of 0.06 m.

The M_R-N_R interaction diagrams for the three amounts of reinforcement are illustrated in Figure 5, together with the lining forces M-N numerically predicted at the end of the construction stage (static, in gray) and at the end of the earthquake (dynamic, in orange). Each point represents the M-N stress state retrieved in correspondence of one node on the tunnel cross section.

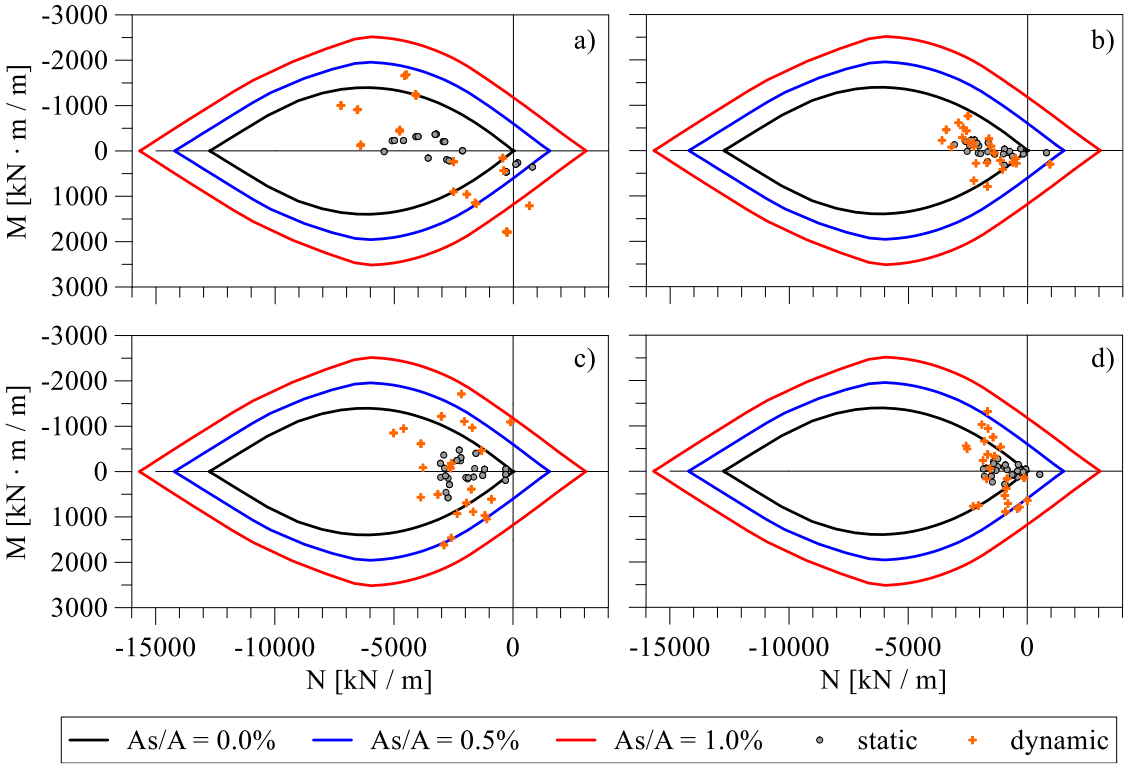

Figure 5: Scatter plot of lining forces at the end of the construction stage (static) and at the end of the earthquake (dynamic) overlaid on three hypothesized M_R-N_R interaction diagrams for p equal to a) 150 m, b) 250 m, c) 350 m, and d) 550 m.

At the end of the static stage, all the analyzed sections are mainly subjected to a compressive stress state (except for some points subjected to tensile stresses). Moving toward the north-west portal of the tunnel (i.e. for increasing distance p), the axial forces tend to reduce, since they range between 0 and -5000 kN/m for p = 150 m, while concentrating in the range between 0 and -2000 kN/m for p = 550 m. Most of the stress state points lie within the M_R-N_R diagram built under the hypothesis of absence of reinforcement (A_S/A=0%), while the totality of the stress state points is within the M_R-N_R diagram for A_S/A=0.5%. In any case, despite the stress state points being very close to the envelopes, they concentrate in the area pertaining to a ductile failure.

The occurrence of the earthquake changes the stress state distribution within each cross section, causing an overall increment of the bending moment, while the axial forces remain in the same order of magnitude at the end of the seismic motion. In this case, despite they are very close to the interaction domain, most of the stress points lie within the M_R-N_R diagram for A_S/A=1%, whereas very few points (specifically in the cross section at the distance of 150 m) are outside the strength domain (Figure 5a), revealing the possible failure of the section. Also in this case, apart from the section at p = 150 m, the stress points concentrate around the ductile failure area.

To evaluate the tunnel damage distribution induced by both the tunnel construction stage and the earthquake occurrence, the numerical results have been interpreted in terms of damage index (DI), defined as the ratio between the actual (M) and the capacity (M_R) bending moment of the cross section. Based on the observation of damages in tunnels due to ground shaking and on the engineering judgement, five damage states were identified by [11] as a function of DI, as reported in Table 3. In the present paper the same classification has been assumed for the estimation of the damage state induced by static actions (i.e. tunnel construction).

Damage state	Ranges of damage index
DS0. None	$M/M_R \leq 1.0$
DS1. Minor/slight	$1 < M/M_R < 1.5$
DS2. Moderate	$1.5 < M/M_R < 2.5$
DS3. Extensive	$2.5 < M/M_R \leq 3.5$
DS4. Collapse	$M/M_R > 3.5$

Table 3: Definition of damage states for the tunnel lining according to [11].

In this work, M is the value of the bending moment numerically predicted at the end of both static and dynamic stage, while M_R is the ultimate bending moment associated with a specific axial force N evaluated through the M_R-N_R interaction diagrams. For a comprehensive evaluation of the response of the tunnel, the damage index has been evaluated retrieving the lining forces for the whole structure. Therefore, the contour map of the DI distribution has been reproduced, showing those portions of the tunnel characterized by a specific damage state. The contour maps of the damage index distribution predicted at the end of the tunnel construction and at the end of the seismic event, for different ratios A_S/A, are reported in Figure 6 and Figure 7, respectively. These contour maps report the distance p from the south-east portal on the x-axis and the polar angle θ on the y-axis, together with the location of the side walls, the crown and the invert arc for a better understanding of the figure.

The results show that, in absence of reinforcement (i.e. A_S/A=0%), several portions of the tunnel would be completely damaged ($M/M_R > 3.5$) already at the end of the construction stage. These portions are mainly concentrated in the crown along the whole tunnel, while only a few areas are located in the invert arc (Figure 6a). The increment of the amount of reinforcement to 0.5% reduces the portions in the crown subjected to damage states, while the invert arc would suffer only from minor damage (Figure 6b). No damage would be observed in the tunnel if the reinforcement percentage is 1% (Figure 6c).

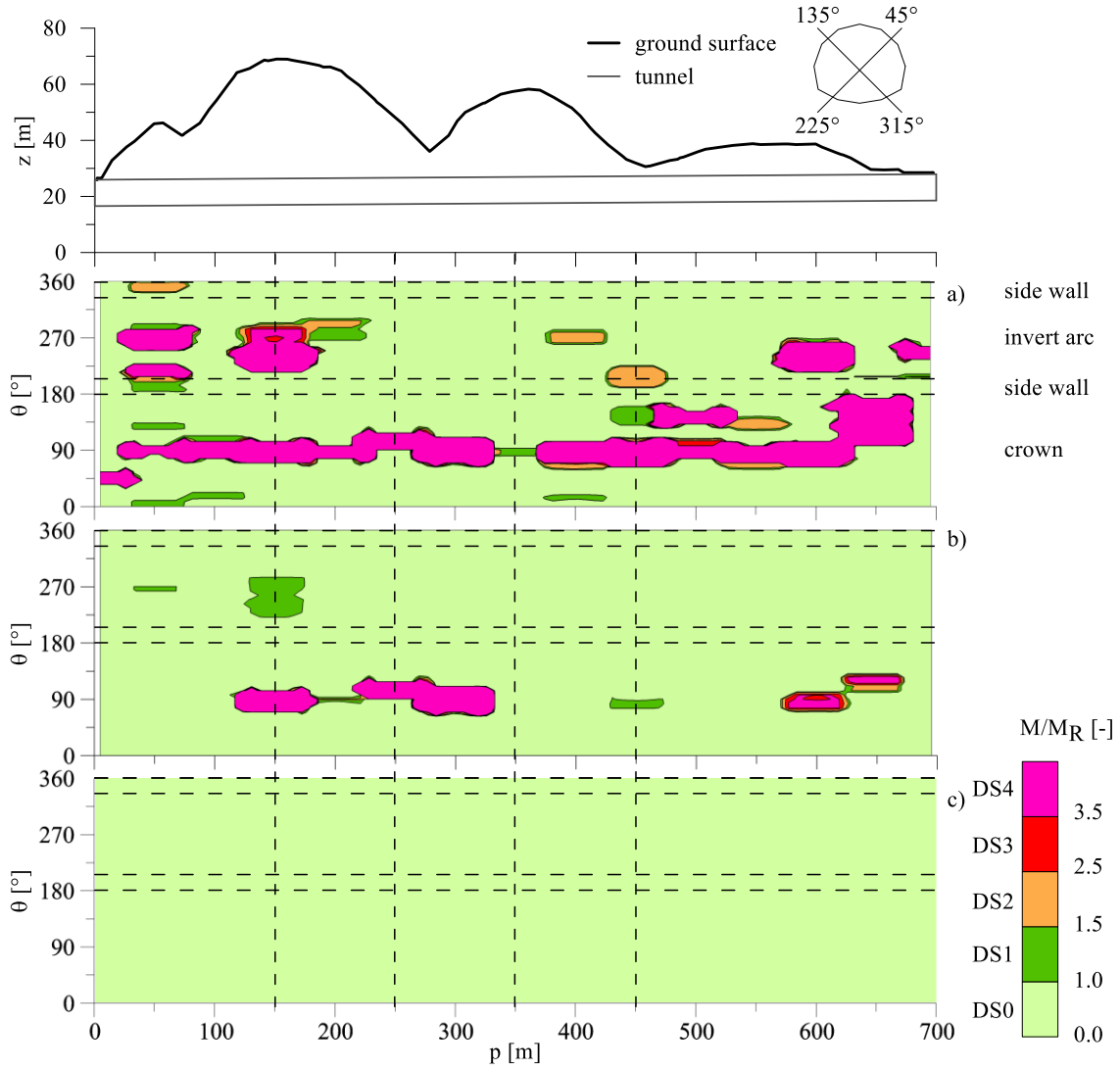

Figure 6: Contour maps of the damage index DI predicted for the right tunnel at the end of the tunnel construction, considering a) A_S/A=0%, b) A_S/A=0.5%, and c) A_S/A=1.0%. The longitudinal section and a typical cross section of the tunnel are shown at the top of the figure.

The occurrence of the earthquake would clearly aggravate the induced damage, depending on the amount of reinforcement. Indeed, a more diffuse damage state might be observed on the tunnel lining both in absence and for a small amount of reinforcement (Figure 7a and b), while for A_S/A=1% minor damage is recognized only at the distance between 100 m and 200 m both in the crown and in the invert arc (Figure 7c). Indeed, in absence of reinforcement, the tunnel would be severely damaged after the seismic event, not only in correspondence of the crown, but also along the side walls and the invert arc. The adoption of a reinforcement percentage equal to 0.5% would not avoid the tunnel from being damaged during the seismic action, since the portions affected by moderate, extensive and collapse damage would be distributed all along the tunnel lining. To exclude any damage to the infrastructure, the ideal reinforcement percentage is 1%.

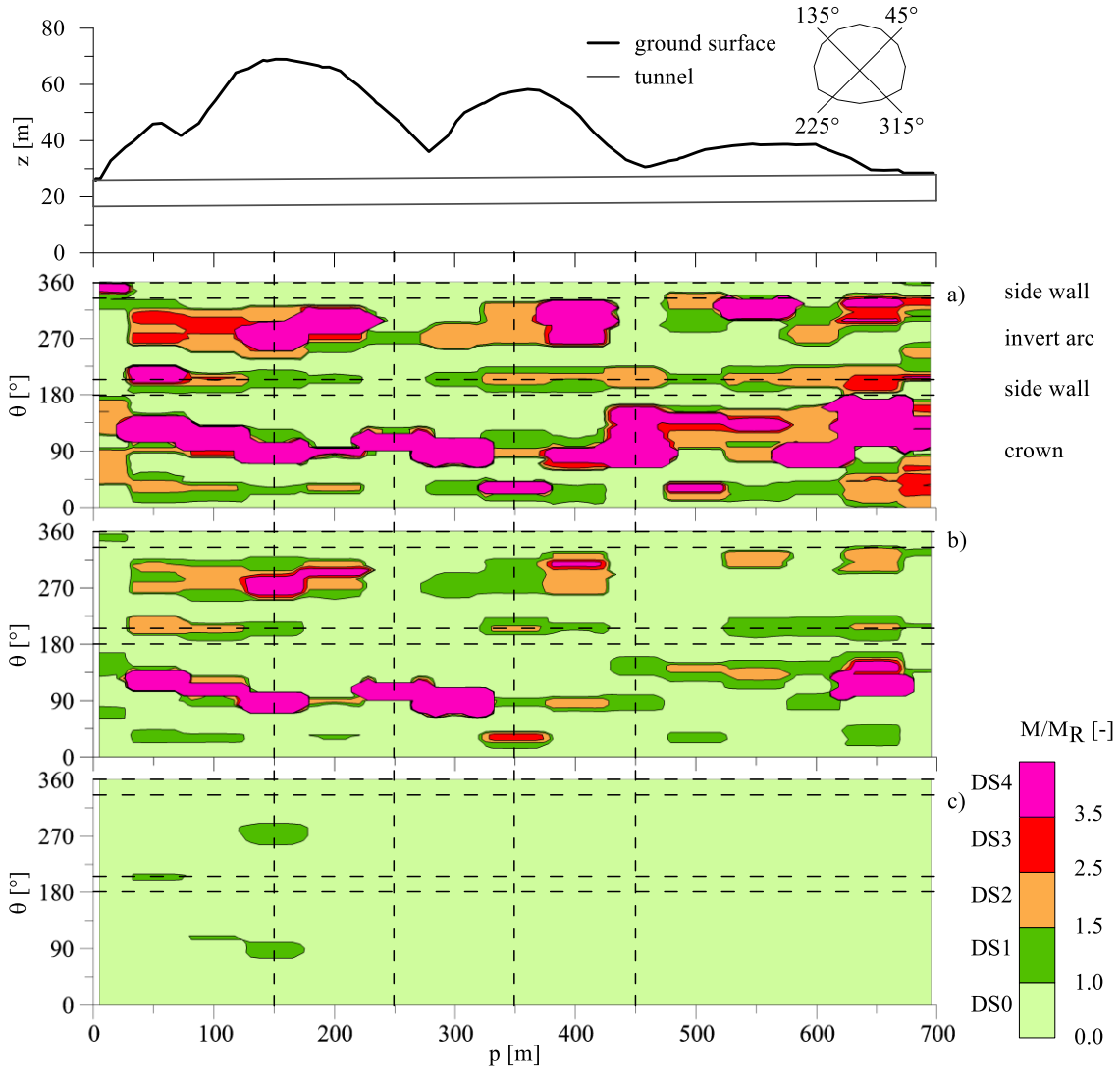

Figure 7: Contour maps of the damage index DI predicted for the right tunnel at the end of the earthquake, considering a) A_S/A=0%, b) A_S/A=0.5%, and c) A_S/A=1.0%. The longitudinal section and a typical cross section of the tunnel are shown at the top of the figure.

5 CONCLUSIONS

The paper presents the results of a 3D FE investigation of the dynamic slope-tunnel interaction of a shallow tunnel located in an area with topographically complex conditions. This analysis has been interpreted to provide indication of the possible damage state induced by the tunnel construction stage and by a seismic action. The study has been conducted with reference to the Alvaro twin-tube tunnel, crossing the toe of the Costa del Canneto area, located in the Basilicata region. In absence of direct information, several assumptions have been made on the tunnel construction strategy, soil dynamic properties, geometry and reinforcement of the tunnel lining. In particular, three different percentages of steel reinforcement have been selected as reasonable values for shallow tunnels. The level of tunnel damage has been estimated as a function of a damage index expressing the exceedance of the lining strength capacity.

The results have been elaborated in terms of contour maps of the damage index estimated along the whole lining, indicating the areas of the tunnel suffering from specific levels of damage at the end of both the static and the dynamic stage. The numerical simulations enlighten that (*i*) the level of damage is strongly dependent on the amount of reinforcement; (*ii*) the tunnel lining would be damaged already after its construction if a small amount of percentage is located in the cross section of the structure; (*iii*) the occurrence of an earthquake would strongly aggravates the level of the induced-damage; (*iv*) no or slight damage would be induced in the lining if the percentage of reinforcement is equal to 1%, representing an optimal condition for the specific case study.

ACKNOWLEDGEMENTS

The authors acknowledge the support received from the PON-MITIGO project (PON Program R&I 2014-2020: MITIGO, ARS01_00964). The second author is grateful for the financial support provided by the European Union – Next Generation EU in the framework of the GRINS – Growing Resilient, Inclusive and Sustainable project (GRINS PE00000018 – CUP E63C22002000002). The last author acknowledges the financial support received from the project "MOST – Sustainable Mobility National Research Center – Spoke 7" (CN_00000023), funded by the European Union – Next Generation EU within the National Recovery and Resilience Plan, Mission 4_2_1.4.

REFERENCES

[1] C. Corbane, U. Hancilar, D. Ehrlich, T. De Groeve, Pan-European seismic risk assessment: a proof of concept using the Earthquake Loss Estimation Routine (ELER). *Bulletin of Earthquake Engineering*, **15**, 1057–1083, 2017. https://doi.org/10.1007/s10518-016-9993-5.

[2] L.T. Cabangon, G. Elia, M. Rouainia, S. Keawsawasvong, The effect of multi-directional seismic loading on the behaviour of tunnels in structured clays. *Computers and Geotechnics*, **160**, 105531, 2023. https://doi.org/10.1016/j.compgeo.2023.105531.

[3] G. Elia, M. Rouainia, Advanced dynamic nonlinear schemes for geotechnical earthquake engineering applications: a review of critical aspects. *Geotechnical and Geological Engineering*, **40**, 3379–3392, 2022. https://doi.org/10.1007/S10706-022-02109-6.

[4] R. Vassallo, M. Mishra, G. Santarsiero, A. Masi, Modeling of Landslide–Tunnel Interaction: the Varco d'Izzo Case Study. *Geotechnical and Geological Engineering*, **37**, 5507-5531, 2019. https://doi.org/10.1007/S10706-019-01020-X.

[5] G. Melidoro, S. Guerricchio, N.L. Melidoro, (In Italian). Comportamento di una galleria stradale al piede di un grande corpo di frana antica. *Geologia Applicata e Idrogeologia*, **31**, 365-371, 1996.

[6] V. Cotecchia, *Relazione geologica e geotecnica per la costruzione di un tratto di linea ferroviaria tra Matera e Ferrandina in funzione di collegamento diretto della Città di Matera alla rete F.S. Progetto Esecutivo: Stazione Ferrandina - Stazione di Matera la Martella*, 1985.

[7] G. Falcone, G. Elia, F. Cafaro, A. di Lernia, Preliminary assessment of the correlation between three-dimensional topography and lining forces induced by earthquakes on

shallow tunnels. *10th European Conference on Numerical Methods in Geotechnical Engineering - NUMGE2023*. London, June 23-26, 2023.

[8] G. Falcone, A. di Lernia, G. Elia, 3D modelling of construction sequences and subsoil heterogeneity effects on the seismic response of shallow tunnels in complex topographical settings. *Computers and Geotechnics*, **180**, 107007, 2025. https://doi.org/10.1016/j.compgeo.2025.107077.

[9] T. Benz, P.A. Vermeer, R. Schwab, A small-strain overlay model. *International Journal for Numerical and Analytical Methods in Geomechanics*, **33**, 25-44, 2009. https://doi.org/10.1002/nag.701.

[10] T. Schanz, P.A. Vermeer, P.G. Bonnier, The hardening soil model: Formulation and verification. *Beyond 2000 in Computational Geotechnics, 1st Edition*, 281–96, 1999.

[11] S.A. Argyroudis, K.D. Pitilakis, Seismic fragility curves of shallow tunnels in alluvial deposits. *Soil Dynamics and Earthquake Engineering*, **35**, 1–12, 2012. https://doi.org/10.1016/j.soildyn.2011.11.004.

[12] ANAS, *Geological report on 2014 site investigations for the Alvaro tunnel site*. Potenza, 2014. (Personal communication).

[13] NTC2018. (In Italian). Norme Tecniche per le Costruzioni, 2018.

[14] M. Del Prete, G. Valentini, Le caratteristiche geotecniche delle argille azzurre dell'Italia sud-orientale in relazione alle differenti situazioni stratigrafiche e tettoniche. *Geologia Applicata e Idrogeologia*, **VI**, 197-215, 1971.

[15] G. Viggiani, J.H. Atkinson, Stiffness of fine-grained soil at very small strains. *Géotechnique*, **45**, 249-65, 1995. https://doi.org/10.1680/geot.1995.45.2.249.

[16] M.B. Darendeli, *Development of a New Family of Normalized Modulus Reduction and Material Damping Curves*. University of Texas, Austin, 2001.

[17] R Brinkgreve, S Kumarswamy, W Swolfs, *PLAXIS 3D Connect Edition V22, Reference manual*, 2022.

[18] K.J. Bathe, *Finite Element Procedures. 2nd Edition.* Upper Saddle River, N.J., Prentice Hall, 1996.

[19] J. Rayleigh, *The theory of sound*. New York, Dover; 1945.